Vegetation Spots and Stripes: Dissipative Structures in Arid Landscapes

OLIVIER LEJEUNE, MUSTAPHA TLIDI, RENÉ LEFEVER

Faculté des Sciences, Campus de la Plaine, CP 231, Université Libre de Bruxelles, Boulevard du Triomphe, B-1050, Bruxelles, Belgium

Received 26 March 2003; accepted 27 October 2003
Published online 12 February 2004 in Wiley InterScience (www.interscience.wiley.com).
DOI 10.1002/qua.10878

ABSTRACT: The large-scale vegetation patterns observed in many arid regions are due to the existence of facilitative and competitive interactions that affect the communal development of plants. For the patterns to form, it is necessary that competitive interactions be of longer range than facilitative interactions. Aridity affects the pattern's symmetry properties. As it increases, one first finds patterns constituted of spots of sparser vegetation, which then transform into an alternation of stripes of sparser and thicker vegetation, and finally into a pattern of vegetation spots separated by bare ground. The model and nonlinear analysis presented below explains the observations.

Key words: vegetation patterns; dissipative structures; symmetry-breaking instabilities; amplitude equations

Introduction

The concept of dissipative structure was discussed for the first time by Ilya Prigogine in a talk on *Structure, Dissipation and Life*, which he gave at an international conference held in Versailles thirty-five years ago [1]. The discussion precedes the discovery of the Belousov–Zhabotinski reaction by western scientists. It also came at a time when many physicochemists were questioning the existence of chemical instabilities and space symmetry–breaking instabilities were phenomena completely unknown in purely dissipative systems. Since those pioneering days, as the current meeting shows, the concept of dissipative structure has thrived—theoretically as well as experimentally—not only in its field of origin, reaction–diffusion systems [2] but in most domains of the natural sciences where the appearance of order and structure involves nonequilibrium exchanges of energy and/or matter. Population dynamics is in this respect a domain of prediliction (see, e.g., Ref. [3]). The vegetation pat-

Correspondence to: R. Lefever; e-mail: rlefever@ulb.ac.be
Contract grant sponsors: Instituts Internationaux de Physique et de Chimie Solvay; Fonds National de la Recherche Scientifique.

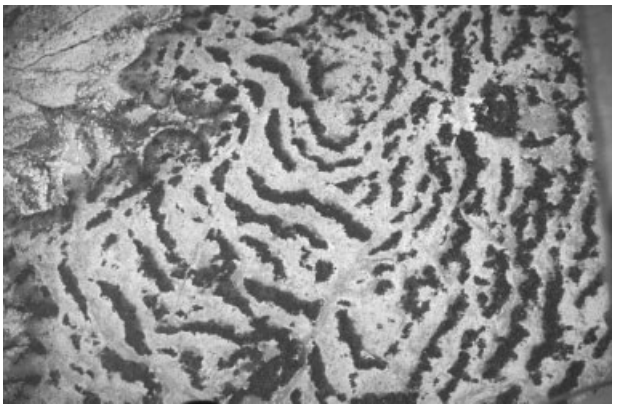

FIGURE 1. Aerial photograph of tiger bush (September 1996) in southwest Niger on a plateau of Banizoumbou site (13°30′ N, 2°40′ E). The bands of dense vegetation (dark) and the separating lanes (bright) are approximately 50 m wide. The vegetation is dominantly constituted of Combretaceae. Annual rainfall: 300–600 mm (courtesy of B. Mougenot).

terns considered below belong to this field of research. They are puzzling, striking examples of large-scale phytosociological organizations controlled by a nonequilibrium symmetry-breaking instability. We see here how changing environmental conditions modulate this instability and explain the various kinds of patterns observed.

Being often undetectable at ground level, the vegetation stripes and arcs found in many arid regions were initially put into evidence with the initial use of aerial photographs in the early 1940s [4]. The organizations appear as bands or arcuate areas of vegetation alternating periodically with sparsely populated areas or even bare ground. They are known under the name of *brousse tigrée* (tiger bush) [5]. They were observed on vast territories of many arid regions of Africa, Australia, North America, and of the Middle East [6, 7]. A typical example of tiger bush from Niger extending over 1 km is reproduced in Figure 1. More recently, spotted patterns made up of either vegetation clearings or clumps also were reported [8].

Some field data from Africa are shown in Table I [9–12]. The pattern wavelength is defined as the sum of the width of densely (or sparsely) populated patches and of their spacing. The phenomenon is not specific to peculiar plants or soils. Vegetation may wholly consist of grasses. The wavelength is in that case of the order of 10 m. When shrubs and trees are involved, the order of magnitude is 100 meters. Moreover, patterns may develop on lands ranging from sandy and silty to clayey. The annual rainfall (50–750 mm) is low with regard to potential evapo-transpiration ($\geq 1.5\ 10^3$ mm). As annual rainfall decreases, the average vegetation density decreases while the pattern wavelength increases [13,

TABLE I
Characteristics of some vegetation patterns observed in Africa.

Region	Vegetation	Patterns		Slope, orientation	Rainfall
British Somaliland [9]	Grass, shrubs, Isolated trees h: 6–10	Arcs, w:	30–40	1:400	70–430
		s:	120–130	Perpendicular	
		l:	500–1000		
		Stripes, w:	80–100	Parallel	
		s:	80–400		
		l:	3000–4000		
Sudan [10, 11]	Grass	Stripes, w:	8–12	1:160 to 1:300	100–400
		s:	20–30	Perpendicular	
	Trees h: 4–5	Arcs, w:	40–50	1:200 to 1:50	
		s:	50–60		
		l:	150–300		
Burkina Faso [12]	Shrubs, trees h: 3–5	Stripes, w:	20–30	1:100 or less	450–600
		s:	30–40	Perpendicular	
		l:	100–500		
		Spots, w:	15–25	Virtually flat	
		s:	40–50		

Abbreviations: h, Height; w, width; s, spacing; l, length (in m). Rainfall is annual (in mm).

14]. Comparing different patterns constituted of the same vegetation indicates that the ground slope can determine the spatial symmetry and/or orientation. Spots are replaced by stripes or arcs; the latter are oriented orthogonally to the slope direction.

Almost all territories where this arid vegetation patterning has been noticed are (or were until recent times) uninhabited. The distribution of rainfall and the underlying bedrock are homogeneous at the scale of the pattern wavelength. Soil differences between areas of thicker and sparser vegetation are primarily differences of organic matter content due to the vegetation itself [6]. An upslope migration of stripes [10, 15] further argues for a dynamical origin. Early explanations call upon water redistribution from scattered to dense vegetation patches through run-off [16, 17]. Yet models postulating that the anisotropy caused by the ground slope is necessary to pattern formation in arid regions [18] are unable to explain the appearance of spatially periodic spots.

The generic evolution equation for the phytomass density [19] that we consider in the following fills this theoretical gap. Indeed, stripes and spots arise via a Turing-like instability [20] that acts even under strictly homogeneous and isotropic environmental conditions. Spatial effects are governed by the balance between positive and negative interactions, which is by now recognized as a determining factor for most plant communities [21]. The pattern wavelength then results from an interplay between short-range facilitation and long-range competition. Recent reaction–diffusion models of plant and water dynamics [22] proposed to explain arid vegetation patterning are based on this spatial symmetry-breaking mechanism.

In the current article, we study how the aridity level influences the formation of vegetation patterns in the absence of environmental anisotropies such as, notably, a ground slope. The minimum and maximum phytomass densities of stripes and spots as well as their stability are determined by using the amplitude equations formalism. The analytical bifurcation diagram of vegetation states as a function of the control parameter measuring water availability is constructed. Pattern selection analysis is in agreement with numerical integration of the kinetic equation. The sequence of spatially periodic states obtained for increasing aridity is: spots of lower density forming a hexagonal lattice, alternating stripes of higher and lower density, and spots of higher density forming an hexagonal lattice.

The Model

The space–time organization of the vegetation is described in terms of the total phytomass density $\rho(\mathbf{r}, t)$ appropriately adimensionalized to be defined on the interval [0, 1]. Admitting that the environment is spatially isotropic, it has been established that the kinetic equation giving the spatio-temporal evolution of the density can be written in partial differential equation form as [23, 24]

$$\frac{\partial \rho}{\partial t} = (1 - \mu)\rho + (\Lambda - 1)\rho^2 - \rho^3 + \frac{1}{2}(L^2 - \rho)\Delta\rho - \frac{1}{8}\rho\Delta^2\rho, \quad (1)$$

where Δ is the two-dimensional Laplacian. This equation applies in the case of water-limited ecosystems when the average phytomass density is low and when the pattern's wavelength is much larger than the size of the plants. Three parameters control the dynamics: (i) the mortality-to-growth rate ratio μ, which increases with the aridity (a drier environment usually implies a lower growth rate and, possibly, higher mortality of the phytomass [25]); (ii) Λ, which fixes the strength of the (anti)-cooperative effects experienced by the plants as a result of their facilitative and competitive interactions; (iii) the ratio L of the spatial ranges over which the facilitative and competitive interactions operate. The most salient feature of Eq. (1) is the fact that the vegetation transport coefficient, $1/2(L^2 - \rho)$, which multiplies the Laplacian term and plays the role of diffusion coefficient, becomes negative when ρ exceeds L. Clearly, the behavior tends to destabilize the spatial uniformity of the vegetation density. In contrast, the factor multiplying the double Laplacian, $-1/8\rho$, also depends on the density but is always negative; it insures that the unbounded growth of local (small) heterogeneities is impossible.

UNIFORM STATIONARY DISTRIBUTIONS

The homogeneous steady states, ρ_s, are the solutions of the cubic polynomial equation $\rho_s[1 - \mu + (\Lambda - 1)\rho_s - \rho_s^2] = 0$. The behavior in terms of the kinetic parameters μ and Λ is sketched in Figure 2. The roots are $\rho_0 = 0$ and

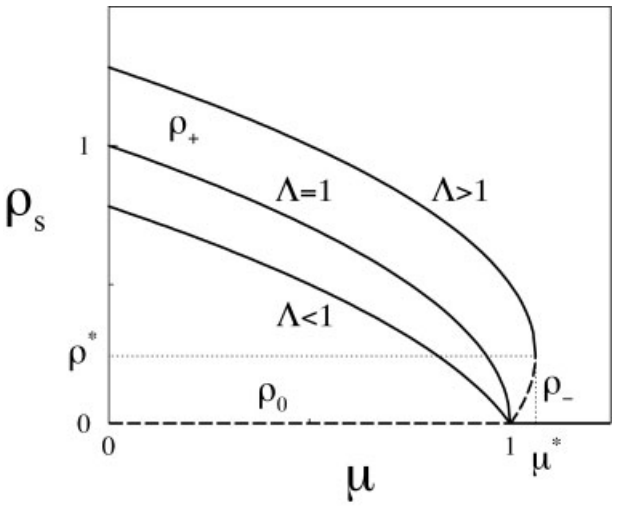

FIGURE 2. Uniform stationary distributions of the phytomass density ρ_s, and their stability with respect to homogeneous perturbations, are plotted against the parameter μ measuring aridity for different values of the vegetation feedback constant Λ. Unstable states are represented by broken lines. As a consequence of the low density approximation, large values of ρ_s obtained in the vicinity of the origin $\mu = 0$ for $\Lambda \neq 1$ are misleading.

$$\rho_{\pm} = \frac{\Lambda - 1 \pm \sqrt{(\Lambda - 1)^2 + 4(1 - \mu)}}{2}. \qquad (2)$$

The branch of trivial solutions, ρ_0, represents territories devoid of vegetation. It always exists but switches from unstable to stable (with respect to homogeneous perturbations) when μ increases beyond one. When the two other solutions, $\rho_{\pm}$, are real and positive, they represent spatially uniform plant distributions. Two cases must be distinguished according to the value of Λ. If $0 < \Lambda \leq 1$, only the branch ρ_+ is meaningful insofar as $0 \leq \mu \leq 1$. If $\Lambda > 1$, the physical part of the branch extends up to the turning point (μ^*, ρ^*) given by $\mu^* = 1 + 1/4(\Lambda - 1)^2$ and $\rho^* = 1/2(\Lambda - 1)$. Besides, the branch ρ_- physically exists in the interval $1 \leq \mu \leq \mu^*$. The branch ρ_+ is stable, whereas the branch ρ_- is unstable.

As the (aridity) value of μ increases, the vegetation evolves toward extinction. For $0 < \Lambda \leq 1$, the decrease of the phytomass density is continuous. Zero density is reached at the switching point $\mu = 1$, where the stable branch ρ_+ crosses the trivial branch ρ_0. Beyond that point, the stable homogeneous steady-state ρ_0 is the only one possible. For $\Lambda > 1$, the decrease is discontinuous and the phytomass density drops from ρ^* to zero at the limit point $\mu = \mu^*$. Indeed, a hysteresis loop and a bistability phenomenon appear in the range $1 \leq \mu \leq \mu^*$: the stable branches ρ_+ and ρ_0 coexist with the intermediate unstable branch ρ_-. When $\mu > \mu^*$, only the trivial state ρ_0 remains possible.

SYMMETRY-BREAKING INSTABILITY

We now look for the conditions under which spatially uniform distributions of vegetation are unstable. As a matter of fact, the only nonzero homogeneous steady state that is stable in the absence of spatial effects, ρ_+, may become unstable with regard to inhomogeneous perturbations. In the Fourier representation, growing modes are characterized by a finite interval of wavenumbers excluding the origin. This domain must exclude very large wavelengths (small wavenumbers) corresponding to quasiuniform distributions and very small wavelengths (large wavenumbers) corresponding to inhomogeneities smaller than the interaction ranges. This Turing kind of symmetry-breaking scenario produces patterns characterized by an intrinsic wavelength determined by the system's dynamics rather than by geometrical factors and/or boundary conditions.

Small amplitude deviations from ρ_+ are governed by Eq. (1) linearized around the reference state. They are expressed in terms of Fourier modes $\exp(\omega_k t + i\mathbf{k} \cdot \mathbf{r})$ in the space of wavevectors $\mathbf{k}$. Taking into account the homogeneous steady state condition $\mu = 1 + (\Lambda - 1)\rho_+ - \rho_+^2$, the dispersion relation obeyed by the eigenvalues ω_k reads

$$\omega_k = \rho_+(\Lambda - 1 - 2\rho_+) - \frac{1}{2}(L^2 - \rho_+)k^2 - \frac{1}{8}\rho_+ k^4. \qquad (3)$$

Given the isotropy of space, it is a real quantity whose value depends only upon the modulus of the wavevectors $k = |\mathbf{k}|$, that is, the wavenumber. According to whether ω_k is negative or positive, the amplitude of the modes of wavelength $\lambda = 2\pi/k$ grows or decreases in the course of time. The first and last terms in the expression for ω_k are always negative, because $\rho_+ > 0$ and $\rho_+ > 1/2(\Lambda - 1)$ [see Eq. (2)]. They insure that fluctuations of arbitrarily small or large wavenumbers are damped, that is $\omega_{k \to 0} < 0$ and $\omega_{k \to \infty} < 0$.

As a function of k, the eigenvalue curves ω_k pass through a maximum at

$$k = k_0 = \sqrt{2\left(1 - \frac{L^2}{\rho_+}\right)}, \tag{4}$$

as soon as the condition $L < \sqrt{\rho_+}$ is realized. Given that ρ_+ does not depend upon L, it is clear that this inequality can always be fulfilled by decreasing the value of L. A modulational instability then occurs, provided that the eigenvalue corresponding to k_0 changes sign and becomes positive. Moreover, because the phytomass density cannot exceed one, pattern formation requires that $L < 1$, or equivalently, that the competition range must extend beyond the facilitation range. This condition is analogous to the condition governing the occurrence of Turing instabilities in reaction–diffusion systems, namely, that inhibitors must diffuse faster than activators.

The homogeneous steady state ρ_+ undergoes a symmetry-breaking bifurcation whenever the phytomass density reaches a critical value ρ_c, satisfying the equation $2\rho_c^2(1 - \Lambda + 2\rho_c) = (L^2 - \rho_c)^2$. At this threshold, the critical wavenumber is $k_c = \sqrt{2(1 - L^2/\rho_c)}$. Beyond the bifurcation point, all modes whose wavenumber belongs to the open interval $]k_-, k_+[$ given by

$$k_\pm = \sqrt{2\left[\left(1 - \frac{L^2}{\rho_+}\right) \pm \sqrt{\left(1 - \frac{L^2}{\rho_+}\right)^2 - 2(1 - \Lambda + 2\rho_+)}\right]} \tag{5}$$

are amplified. Indeed, the dispersion relation ω_k assumes zero value at wavenumbers k_- and k_+ but positive values in between. The domain of instability includes the wavenumber of the fastest-growing modulation, $k_- < k_0 < k_+$. The critical wavenumber corresponds to the situation where the lower and upper bounds of the interval merge, $k_c = k_- = k_+$.

The occurrence of the symmetry-breaking instability is illustrated in Figure 3. The wavenumbers k associated with growing Fourier modes are shown in terms of the homogeneous steady-state $\rho_s = \rho_+$. When the phytomass density is high enough, $\rho_s > \rho_c$, the uniform distribution of vegetation is stable. As aridity increases, and subsequently the phytomass density decreases, $\rho_c' < \rho_s < \rho_c$, the homogeneous state becomes unstable. Because $k_c' < k_c$, the wavelength of the vegetation patterns increases under those conditions, in agreement with in situ observations. When the phytomass density becomes too low, $\rho_s < \rho_c'$, stability is restored. When there is no hysteresis loop, $\Lambda \leq 1$, the domain of instability is bounded as a rule by an upper and lower critical point, ρ_c and ρ_c'. Whereas in the bistable regime, $\Lambda > 1$, the branch ρ_+ may be unstable down to ρ^* (see Fig. 2).

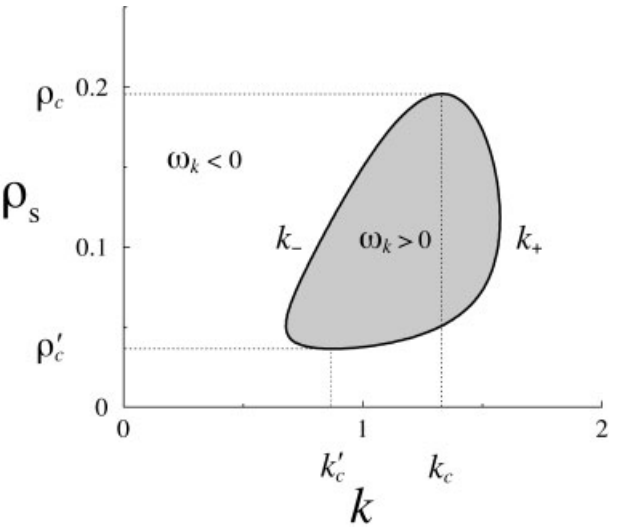

FIGURE 3. The domain of instability for $\Lambda = 1$ and $L = 0.15$ is represented by a gray shaded area in the (k, ρ_s)-plane. As the phytomass density $\rho_s = \rho_+$ decreases, the succession stability–instability–stability is the following: first, all modes decrease when $\rho_s > \rho_c$; second, there appears a critical wavenumber k_c for $\rho_s = \rho_c$, so that modes of wavenumber between k_- and k_+ grow when $\rho_c' < \rho_s < \rho_c$; third, there appears another critical wavenumber k_c' for $\rho_s = \rho_c'$, so that all modes decrease again when $\rho_s < \rho_c'$.

Bifurcation Analysis

We implement here the truncated Fourier series expansion [26, 27]*: the asymptotic form of the solution is postulated as a function of the modes composing the spatial symmetry of the final pattern. The partial differential equation reduces for long times to a set of ordinary differential equations describing the dynamics of the unstable modes. When there is bistability, $\Lambda > 1$, it has been shown

* Nonlinear analysis is based on the formalism of amplitude equations. Classically, the equations are obtained by an expansion around the critical symmetry-breaking instability point. Distance from criticality is then the expansion smallness parameter [26]. When, like here, there are two bifurcation points, the method satisfactorily applies only under the restricted conditions where these two points nearly coalesce.

that the branches of spatially periodic solutions may extend beyond the branches of nonzero homogeneous steady states [24]. Hereafter, only the monostable regime, $\Lambda \leq 1$, is considered. For each spatial symmetry, there is a single branch of pattern solutions connecting continuously the two bifurcation points that are related to distinct critical values of the control parameter and of the wavenumber.

The solution of kinetic Eq. (1) is assumed to behave asymptotically as

$$\rho(\mathbf{r}, t) = \psi_0(t) + \sum_{j=1}^{N} \frac{1}{2} [\psi_j(t) e^{i(\phi_j(t) + \mathbf{k}_j \cdot \mathbf{r})} + c.c.], \quad (6)$$

where c.c. denotes the complex conjugate. The homogeneous term ψ_0 is the average phytomass density. It depends on time and is not merely equal to the steady state $\rho_s = \rho_+$. The time dependence of the inhomogeneous terms appears in the amplitudes, ψ_j, and phases, ϕ_j, of the Fourier modes. The wavevectors $\mathbf{k}_j$ determining the spatial periodicity and symmetry of the pattern are fixed. Their orientation as a whole for an arbitrarily large isotropic system depends on the initial condition and not on the kinetic parameters. On the other hand, their modulus is equal to the wavenumber of the fastest-growing modes, $|\mathbf{k}_j| = k_0$ [see Eq. (4)]. In practice, solely the cases of stripes, $N = 1$, and of spots occupying the vertices of hexagons, $N = 3$, are treated. As a matter of fact, other spatial symmetries are observed neither in numerical simulations nor in arid vegetation patterns.

STRIPES

Stripes are described by a single wavevector $\mathbf{k}_1$. The identity obtained by replacing Eq. (6) for $N = 1$ in kinetic Eq. (1) must hold true in all space. Therefore, for each complex exponential function of space, the total factor on one side is equated to the corresponding factor on the other side. The real and imaginary parts on both sides of each resulting equation are then identified. Recalling that $|\mathbf{k}_1| = k_0$ and $\mu = 1 + (\Lambda - 1)\rho_+ - \rho_+^2$, it leads to

$$\frac{d\psi_0}{dt} = \psi_0 \Big[\rho_+(1 - \Lambda + \rho_+) + (\Lambda - 1)\psi_0 - \psi_0^2 - \frac{3}{2}\psi_1^2 \Big] + \tilde{\beta}\psi_1^2, \quad (7)$$

$$\frac{d\psi_1}{dt} = \psi_1 \Big[\tilde{\alpha} + (\Lambda - 1 + 2\tilde{\beta})\psi_0 - 3\psi_0^2 - \frac{3}{4}\psi_1^2 \Big], \quad (8)$$

$$\psi_1 \frac{d\phi_1}{dt} = 0, \quad (9)$$

when harmonic contributions are not taken into account. The new coefficients are

$$\tilde{\alpha} = \rho_+(1 - \Lambda + \rho_+) - \frac{1}{2} L^2 k_0^2, \quad (10)$$

$$\tilde{\beta} = \frac{1}{2}(\Lambda - 1) + \frac{1}{4} k_0^2 - \frac{1}{16} k_0^4. \quad (11)$$

The homogeneous term, ψ_0, and the amplitude, ψ_1, evolve independently of the phase, ϕ_1.

Two approximations are applied to this evolution: (i) the average density, ψ_0, is assumed to vary quickly compared with the amplitude of the spatial modulation, ψ_1, so that the solution ψ_0 canceling out the right side of Eq. (7) can be replaced in Eq. (8); (ii) supposing that ψ_1 is small ($\psi_1 \ll 1$), ψ_0 is written as a Taylor series expansion

$$\psi_0(t) = c_0 + c_2\psi_1(t)^2 + c_4\psi_1(t)^4 + \cdots. \quad (12)$$

The coefficients c_j are determined by substituting this expression of ψ_0 in the right side of Eq. (7) and by equating to zero each factor multiplying the increasing powers of ψ_1. The coefficient c_0 is calculated from the first equality, the coefficient c_2 is calculated with the help of the result from the second equality, and so on

$$c_0 = \rho_+, \quad c_2 = \frac{L^4 - (2\Lambda - 1)\rho_+^2 + 6\rho_+^3}{4\rho_+^3(\Lambda - 1 - 2\rho_+)}, \ldots. \quad (13)$$

The homogeneous term ψ_0 is equal to the steady-state ρ_+ in first approximation. Depending on the sign of the correction, that may change when varying the values of the kinetic parameters, patterning go along with a decrease or an increase of the mean phytomass density.

After replacing Eqs. (12) and (13) in Eq. (8), and neglecting terms of higher order than cubic, the latter becomes

$$\frac{d\psi_1}{dt} = \psi_1[\alpha - \gamma\psi_1^2]. \quad (14)$$

There is no quadratic term, because the symmetry $\psi_1 \to -\psi_1$ ($\phi_1 \to \phi_1 \pm \pi$) of stripes must be verified. The coefficients of this amplitude equation are

$$\alpha = \frac{L^4 - 2L^2\rho_+ + (2\Lambda - 1)\rho_+^2 - 4\rho_+^3}{2\rho_+}, \quad (15)$$

$$\gamma = \frac{3}{4} - \frac{\begin{array}{c}(L^4 - (4\Lambda - 3)\rho_+^2 + 12\rho_+^3) \\ \times (L^4 - (2\Lambda - 1)\rho_+^2 + 6\rho_+^3)\end{array}}{8\rho_+^5(1 - \Lambda + 2\rho_+)}. \quad (16)$$

The coefficient of the linear term is the largest eigenvalue of the dispersion relation, $\alpha = \omega_{k=k_0}$. It assumes the value zero at the points of bifurcation and is positive in the domain of instability. The coefficient of the cubic term, γ, accounts for nonlinear effects without which a finite nonzero steady state cannot exist.

Indeed, the stationary amplitudes, ψ_{1s}, are the positive constant solutions of Eq. (14). Their expressions are

$$\psi_{1s}^U = 0 \quad \text{and} \quad \psi_{1s}^S = \sqrt{\frac{\alpha}{\gamma}}. \quad (17)$$

The first solution, ψ_{1s}^U, corresponds to a uniform distribution of the phytomass; its existence is restricted to the one of ρ_+. The second solution, ψ_{1s}^S, represents spatially periodic stripes of vegetation; its condition of existence is $\alpha/\gamma > 0$. Moreover, the stationary phase, ϕ_{1s}, is a constant solution of Eq. (9). It depends only upon the initial condition in the case of ψ_{1s}^S and is undefined in the case of ψ_{1s}^U. In the vicinity of a bifurcation point, the solution ψ_{1s}^S behaves as the square root of the distance from that critical point.

The stability of the stationary amplitudes, ψ_{1s}, is determined by Eq. (14) linearized around the steady states. The solution of each linear equation is proportional to $\exp(\sigma t)$, where σ is the eigenvalue. Its expressions are

$$\sigma^U = \alpha \quad \text{and} \quad \sigma^S = -2\alpha. \quad (18)$$

Hence, the solution ψ_{1s}^U is stable when $\alpha < 0$ and unstable when $\alpha > 0$. Inversely, the solution ψ_{1s}^S is stable when $\alpha > 0$, that is $\gamma > 0$, whereas it is unstable when $\alpha < 0$, that is $\gamma < 0$. If $\gamma > 0$, stripes arise when the homogeneous steady state ρ_+ loses its stability. They are stable with regard to perturbations of small amplitude respecting their spatial symmetry. The bifurcation is called supercritical. If $\gamma < 0$, unstable stripes appear when the state ρ_+ becomes stable; the bifurcation is subcritical. Higher-order terms in Eq. (14) are then required to account for stable stripes. This situation is discarded hereafter.

HEXAGONS

They are described by three wavevectors of modulus k_0 forming three angles of $2\pi/3$. The wavevectors are characterized by the equality $\mathbf{k}_1 + \mathbf{k}_2 + \mathbf{k}_3 = \mathbf{0}$. Replacing Eq. (6) for $N = 3$ in kinetic Eq. (1) and proceeding as in the case of stripes, the resulting amplitude equations for hexagons are

$$\frac{d\psi_1}{dt} = \alpha\psi_1 - \beta\cos(\Phi)\psi_2\psi_3 - \gamma\psi_1^3 - \gamma'\psi_1(\psi_2^2 + \psi_3^2), \quad (19)$$

$$\frac{d\Phi}{dt} = \beta\frac{\psi_1^2\psi_2^2 + \psi_1^2\psi_3^2 + \psi_2^2\psi_3^2}{\psi_1\psi_2\psi_3}\sin(\Phi), \quad (20)$$

where $\Phi = \phi_1 + \phi_2 + \phi_3$ is the total phase. The last equation is the adding up of the equations for the different phases. It is valid only when all amplitudes assume values distinct from zero. The equations for ψ_2 and ψ_3 are obtained from the first equation by cyclic permutations of the subscripts. The new coefficients are

$$\beta = \frac{L^4 - (2\Lambda - 1)\rho_+^2 + 6\rho_+^3}{2\rho_+^2}, \quad (21)$$

$$\gamma' = \frac{3}{2} - \frac{\begin{array}{c}(L^4 - (4\Lambda - 3)\rho_+^2 + 12\rho_+^3) \\ \times (L^4 - (2\Lambda - 1)\rho_+^2 + 6\rho_+^3)\end{array}}{8\rho_+^5(1 - \Lambda + 2\rho_+)}. \quad (22)$$

In contrast to the case of stripes, the amplitude equations for hexagons involve quadratic terms that break the symmetry $\psi_j \to -\psi_j$ ($j = 1, 2, 3$). Consequently, the variations of the amplitudes and of the total phase are interdependent.

The steady states can be divided into two classes. The first one includes the solutions with at least one stationary amplitude, ψ_{js}, equal to zero

$$\psi_{1s}^U = \psi_{2s}^U = \psi_{3s}^U = 0, \quad (23)$$

$$\psi_{1s}^{S} = \sqrt{\frac{\alpha}{\gamma}} \quad \psi_{2s}^{S} = \psi_{3s}^{S} = 0, \tag{24}$$

for which the stationary total phase, Φ_s, is undefined. The former solution represents the homogeneous steady state of the phytomass density ρ_+. Its stability is determined by the eigenvalues $\sigma_1^{UI} = \sigma_2^{UI} = \sigma_3^{UI} = \alpha$. Hence, it is stable when $\alpha < 0$ and unstable when $\alpha > 0$. The latter solution corresponds to the stripes got previously [see Eq. (17)]. The second class encompasses the steady states with no amplitude equal to zero. In that case, the constant solutions of Eq. (20) are

$$\Phi_s = \begin{cases} 0 \\ \pi. \end{cases} \tag{25}$$

Steady states with different amplitudes, corresponding to intermediate patterns between stripes and hexagons, are disregarded because they are always unstable.

For $\Phi_s = 0$, the stationary amplitudes of hexagons are

$$\psi_{1\pm}^{H_0} = \psi_{2\pm}^{H_0} = \psi_{3\pm}^{H_0} = \frac{-\beta \pm \sqrt{\beta^2 + 4\alpha(\gamma + 2\gamma')}}{2(\gamma + 2\gamma')} \equiv \psi_{\pm}^{H_0}. \tag{26}$$

Assuming $\gamma > 0$, and hence $\gamma' > 0$ because $\gamma' > \gamma$, hexagons of type 0 appear in a subcritical way when $\beta < 0$. As a matter of fact, the upper solution, $\psi_+^{H_0}$, exists as soon as $\alpha > -1/4\beta^2/(\gamma + 2\gamma')$, whereas the existence of the lower solution, $\psi_-^{H_0}$, is limited to $-1/4\beta^2/(\gamma + 2\gamma') < \alpha < 0$. When $\beta > 0$, the pattern H_0 appears in a supercritical way. Only the upper solution exists on condition that $\alpha > 0$. The stability of this hexagonal pattern is determined by the eigenvalues

$$\sigma_{1\pm}^{H_0} = -2\alpha + \beta\psi_{\pm}^{H_0}, \tag{27}$$

$$\sigma_{2\pm}^{H_0} = \sigma_{3\pm}^{H_0} = 2\,\frac{-\alpha(\gamma - \gamma') + \beta(2\gamma + \gamma')\psi_{\pm}^{H_0}}{\gamma + 2\gamma'}, \tag{28}$$

$$\sigma_{4\pm}^{H_0} = \beta\psi_{\pm}^{H_0}. \tag{29}$$

Given its condition of existence, the lower solution $\psi_-^{H_0}$ is always unstable because $\sigma_{1-}^{H_0} > 0$. On the other hand, the upper solution $\psi_+^{H_0}$ is unstable when $\beta > 0$ because then $\sigma_{4+}^{H_0} > 0$. Given that $\sigma_{1+}^{H_0} < 0$, it is stable or unstable when $\beta < 0$, depending on whether $\sigma_{2,3+}^{H_0} < 0$ or $\sigma_{2,3+}^{H_0} > 0$, because then $\sigma_{4+}^{H_0} < 0$. Properties of hexagons for $\Phi_s = \pi$ are deduced from above discussion simply by changing β into $-\beta$.

PATTERN SELECTION

Stripes and hexagons of type 0 or π can be at the same time linearly stable with regard to perturbations respecting their own spatial symmetry. Hence, the analysis of the relative stability between stripes and hexagons is necessary to solve the problem of pattern selection. This linear analysis is possible because stripes are particular solutions of the amplitude equations for hexagons. The stability of stripes with respect to perturbations of small amplitude having an hexagonal symmetry is determined by the three eigenvalues

$$\sigma_1^S = -2\alpha, \tag{30}$$

$$\sigma_2^S = \frac{\alpha}{\gamma}(\gamma - \gamma') + \beta\cos(\Phi_s)\sqrt{\frac{\alpha}{\gamma}}, \tag{31}$$

$$\sigma_3^S = \frac{\alpha}{\gamma}(\gamma - \gamma') - \beta\cos(\Phi_s)\sqrt{\frac{\alpha}{\gamma}}. \tag{32}$$

The last two eigenvalues both depend on the stationary total phase Φ_s that is equal to 0 or π. However, the stability of stripes is independent of the type of hexagonal perturbation. Indeed, switching from one type to the other amounts to change the sign of $\cos(\Phi_s)$ and therefore to interchange σ_2^S with σ_3^S. In the supercritical case being considered, $\alpha > 0$ and $\gamma > 0$, the first eigenvalue is negative, $\sigma_1^S < 0$. The sum of the two other eigenvalues is negative, $\sigma_2^S + \sigma_3^S = \alpha/\gamma(\gamma - \gamma') < 0$, because $\gamma < \gamma'$. Consequently, at least one of them is negative. Their product, that is, $\sigma_2^S\sigma_3^S = \alpha/\gamma[\alpha/\gamma(\gamma - \gamma')^2 - \beta^2]$ as $\cos(\Phi_s)^2 = 1$, may change sign. If the product is negative, one of the eigenvalues is positive and the other is negative; if it is positive, both of them are negative. In conclusion, stripes are linearly stable with regard to hexagonal perturbations of both types when $\alpha > \beta^2\gamma/(\gamma - \gamma')^2$ and are unstable otherwise.

The results of the nonlinear analysis are summed up in the bifurcation diagram of Figure 4. The maximum and minimum phytomass densities for each kind of pattern are given as a function of μ for fixed values of Λ and L. In the monostable regime being studied, $\Lambda \leq 1$, there are two critical points of bifurcation. At $\mu = \mu_c$, hexagons of type π appear in

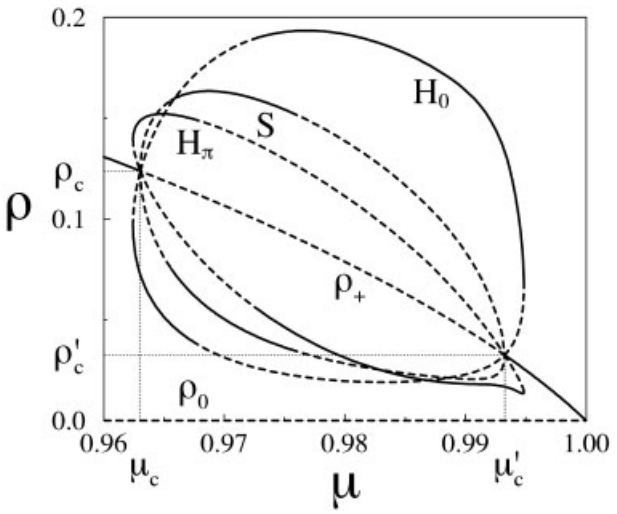

FIGURE 4. The stationary states of the amplitude equations are plotted versus the parameter μ that measures aridity. Parameter values used are $\Lambda = 0.825$ and $L = 0.1$. Broken lines correspond to unstable solutions. For $\mu = 0.965$, only hexagons of type π are stable (H_π). For $\mu = 0.97$, only stripes are stable (S). For $\mu = 0.98$, only hexagons of type 0 are stable (H_0).

a subcritical way, whereas hexagons of type 0 appear in a supercritical way; at $\mu = \mu_c'$, it is the opposite. On the other hand, stripes appear in a supercritical way at both points. As μ increases with aridity, the pattern sequence is H_π–S–H_0. The stability properties then vary as follows: (i) H_π is the only stable pattern; (ii) the patterns H_π and S are both stable; (iii) S is the only stable pattern; (iv) the patterns S and H_0 are both stable; (v) H_0 is the only stable pattern. Subcritical patterns can be initiated from the stable homogeneous steady state ρ_+ only by perturbations of large enough amplitude; that is the case of H_π when $\mu < \mu_c$ and also the case of H_0 when $\mu > \mu_c'$.

NUMERICAL INTEGRATION

The kinetic Eq. (1) is integrated numerically in a square-shaped domain subjected to periodic boundary conditions. The initial condition is chosen to be an unstable homogeneous steady state of the phytomass density, ρ_+, perturbed by some small amplitude random noise. The noise stands for the numerous more or less random environmental factors that disturb the uniformity of natural mediums. The factors may be beneficial to vegetation (animal excreta, plant litter, etc.) or detrimental (fire, grazing, etc.). In the course of time, the density evolves toward a stationary and spatially periodic pattern. The symmetry and amplitude properties depend on the value of the parameters kept fixed and not on the geometry or boundary conditions of the system. As a result of isotropy, the orientation of the pattern is determined only by the initial condition.

The change of pattern when the parameter μ increases with aridity is reported in Figure 5. The interaction susceptibility ratio Λ and the interaction range ratio L are kept constant. The first pattern, H_π, consists of spots of lower density that are distributed on a spatially periodic lattice of hexagonal

FIGURE 5. Three different kinds of patterns are obtained for increasing values of the parameter μ measuring aridity. Parameter values used are $\Lambda = 0.825$ and $L = 0.1$. Black corresponds to the highest phytomass density. (H_π) For $\mu = 0.965$, the density forms hexagons of type π. (S) For $\mu = 0.97$, it forms zigzag stripes. (H_0) For $\mu = 0.98$, it forms hexagons of type 0.

TABLE II
Comparison of analytical and numerical results.[a]

	ρ_{min}		ρ_{max}	
Patterns	Analytical	Numerical	Analytical	Numerical
H_π	0.051	0.057	0.152	0.149
S	0.050	0.048	0.163	0.165
H_0	0.031	0.024	0.192	0.196

[a] The minimum and maximum phytomass densities, ρ_{min} and ρ_{max}, of the simulated patterns H_π, S, and H_0 shown in Figure 5 are compared with the corresponding values of the analytic bifurcation diagram given in Figure 4. Considering the amplitude, $\rho_{max} - \rho_{min}$, the relative deviation between the numerical and analytical values is less than 10% in each case.

symmetry. The next pattern, S, is made of stripes of lower density that alternate periodically in space with stripes of higher density. The last pattern, H_0, is composed of spots of higher density that are arranged according to a hexagonal lattice. The wavelength, determined by the distance separating two successive areas of lower or higher density, is nearly equal to $\lambda = 2\pi/k_0$, given Eq. (4). The spatial symmetry of the simulated patterns is correctly predicted by nonlinear analysis (see the bifurcation diagram of Fig. 4). Numerical and analytical extreme values of the phytomass density are confronted in Table II for each pattern.

When aridity increases, round spots of sparser vegetation first appear in the initially uniform distribution. They then merge to form stripes of sparser and thicker vegetation. Finally, the latter split up into round spots of thicker vegetation. Unlike other models [18], vegetation stripes may occur in isotropic environments, to account for the observation of such patterns on virtually flat territories [5, 13]. Besides stripes, the model generates hexagonal spotted patterns. Vegetation covers regularly punctuated by clearings were observed in West Africa [12]. The spots show a marked dominant wavelength, but hexagonal symmetry is rare. During pattern formation, the wavelength is expected to establish more quickly than the spatial symmetry. Hence, there may not have been enough time to allow the emergence of an hexagonal symmetry.

Discussion

Arid vegetation patterning is interpreted as the outcome of a symmetry-breaking mechanism that works even if the environment is strictly homogeneous and isotropic. Small inherent variations of the vegetation cover are amplified into contrasting large patches of higher and lower phytomass density. This interpretation breaks away from the prevalent view in plant ecology according to which vegetation patterns are transient or ever changing in the absence of stable environmental inhomogeneities [28]. The spatial periodicity results from an interplay between short-range facilitative and long-range competitive plant interactions. The new view is supported by field investigations. Indeed, aerial parts of established plants have positive effects on the growth of nearby plants by providing protection primarily against evapotranspiration [29, 30]. On the other hand, superficial roots are known to track scarce water far beyond the limits of epigenous parts [30, 31]. Hence, the range of negative effects is larger than the one of positive influences. For trees and shrubs, the canopy-to-rhizosphere radius ratio may be as small as 1/10.

In agreement with in situ measures, the predicted wavelength is a decreasing function of the average phytomass density. The model also accounts for a minimal and maximal aridity level below and above which patterning does not occur, as observed along a South–North transect in Niger [32]. As annual rainfall decreases, the pattern is first spotted, then striped, and finally spotted again. However, spots correspond to vegetation clearings in the first case, whereas they correspond to vegetation clumps in the second case. Contrary to a common opinion in the literature [7, 16], anisotropy such as a ground slope is not required for stripe formation. The hexagonal symmetry of spotted patterns, although always obvious in long run simulations, is not often detected in the field [12]. A possible explanation is that the observed patterns are far from having reached an asymptotic state [33]. From a more general standpoint, the theory contributes to establish a relation between the structure of individuals (size of below and above ground parts) and the spatial organization of the plant community (wavelength, symmetry).

ACKNOWLEDGMENTS

The support of the Instituts Internationaux de Physique et de Chimie Solvay is acknowledged. One of the authors (O. L.) is chargé de recherche and another author (M. T.), chercheur qualifié at the Fonds National de la Recherche Scientifique (F.N.R.S.) of Belgium.

References

1. Prigogine, I. Structure, Dissipation and Life. In Theoretical Physics and Biology; Marois, M., Ed.; North Holland: New York, 1969. pp 23–52.
2. Glansdorff, P.; Prigogine, I. Thermodynamic Theory of Structure, Stability and Fluctuations; Wiley-Interscience: New York, 1971.
3. Murray, J. D. Biomathematics Texts, Vol. 19: Mathematical Biology; Springer-Verlag: Berlin, 1989.
4. Macfadyen, W. A. Geogr J 1950, 116, 199.
5. Clos-Arceduc, M. Bull Inst Afr noire Sér A 1956, 18, 677.
6. White, L. P. J Ecol 1971, 59, 615.
7. Valentin, C.; d'Herbès, J. M.; Poesen, J. Catena 1999, 37, 1.
8. (a) Aguiar, M. R.; Sala, O. E. TREE 1999, 14, 273; (b) Couteron, P. Int J Remote Sens 2002, 23, 3407.
9. (a) Boaler, S. B.; Hodge, C. A. H. J Ecol 1962, 50, 465; (b) Boaler, S. B.; Hodge, C. A. H. J Ecol 1964, 52, 511.
10. Worrall, G. A. J Soil Sci 1959, 10, 34.
11. Wickens, G. E.; Collier, F. W. Geoderma 1971, 6, 43.
12. Couteron, P.; Lejeune, O. J Ecol 2001, 89, 616.
13. White, L. P. J Ecol 1970, 58, 549.
14. d'Herbès, J. M.; Valentin, C.; Thiéry, J. M. In Fonctionnement et Gestion des Écosystèmes Forestiers Contractés Sahéliens; d'Herbès, J. M.; Ambouta, J. M. K.; Peltier, R., Eds.; John Libbey Eurotext: Paris, 1997. p 131.
15. (a) Tongway, D. J.; Ludwig, J. A. Aust J Ecol 1990, 15, 23; (b) Montaña, C. J Ecol 1992, 80, 315.
16. Greig-Smith, P. J Ecol 1979, 67, 755.
17. Wilson, J. B.; Agnew, A. D. Q. Adv Ecol Res 1992, 23, 263.
18. (a) Mauchamp, A.; Rambal, S.; Lepart, J. Ecol Mod 1994, 71, 107; (b) Thiéry, J. M.; d'Herbès, J. M.; Valentin, C. J Ecol 1995, 83, 497; (c) Dunkerley, D. L. Plant Ecol 1997, 129, 103; (d) Klausmeier, C. A. Science 1999, 284, 1826.
19. (a) Lefever, R.; Lejeune, O. Bull Math Biol 1997, 59, 263; (b) Lejeune, O.; Couteron, P.; Lefever, R. Acta Oecol 1999, 20, 171.
20. (a) Turing, A. M. Phil Trans Roy Soc Lond Ser B 1952, 237, 37.
21. (a) Bertness, M. D.; Yeh, S. M. Ecology 1994, 75, 2416; (b) Berkowitz, A. R.; Canham, C. D.; Kelly, V. R. Ecology 1995, 76, 1156; (c) Callaway, R. M.; Walker, L. R. Ecology 1997, 78, 1958; (d) Holmgren, M.; Scheffer, M. S.; Huston, M. A. Ecology 1997, 78, 1966.
22. (a) von Hardenberg, J.; Meron, E.; Shachak, M.; Zarmi, Y. Phys Rev Lett 2001, 87, 198101; (b) Okayasu, T.; Aizawa, Y. Prog Theor Phys 2001, 106, 705; (c) Rietkerk, M.; Boerlijst, M. C.; van Langeveld, F.; HilleRisLambers, R.; van de Koppel, J.; Kumar, L.; Prins, H. H. T.; de Roos, A. M. Am Nat 2002, 160, 524.
23. Lejeune, O. PhD Thesis 1999, University of Brussels.
24. Lefever, R.; Lejeune, O.; Couteron, P. IMA Volumes in Mathematics and its Applications, Vol. 121: Mathematical Models for Biological Pattern Formation; Maini, P. K.; Othmer, H. G., Eds.; Springer: New York, 2000. p 83.
25. (a) Fowler, N. Annu Rev Ecol Syst 1986, 17, 89; (b) Kadmon, R. J Ecol 1995, 83, 253.
26. Manneville, P. Dissipative Structures and Weak Turbulence; Academic Press: New York, 1990.
27. (a) Malomed, B. A. Phys Rev A 1992, 45, 1009; (b) Dewel, G.; Métens, S.; Hilali, M'F.; Borckmans, P. Phys Rev Lett 1995, 74, 4647.
28. Pärtel, M.; Zobel, M.; Zobel, K.; van der Maarel, E. J Veg Sci 1996, 7, 19.
29. Vetaas, O. R. J Veg Sci 1992, 3, 337.
30. Belsky, A. J. Ecology 1992, 75, 922.
31. Martens, S. N.; Breshears, D. D.; Meyer, C. W.; Barnes, F. J. J Veg Sci 1997, 8, 655.
32. Ambouta, J. M. K. In Fonctionnement et Gestion des Écosystèmes Forestiers Contractés Sahéliens; d'Herbès, J. M.; Ambouta, J. M. K.; Peltier, R., Eds.; John Libbey Eurotext: Paris, 1997. p 41.
33. Sprugel, D. G. Biol Conserv 1991, 58, 1.